



HAL
open science

Numerical study of laser energy effects on density transition injection in laser wakefield acceleration

F Massimo, Agustin Lifschitz, C. Thaury, Victor Malka

► **To cite this version:**

F Massimo, Agustin Lifschitz, C. Thaury, Victor Malka. Numerical study of laser energy effects on density transition injection in laser wakefield acceleration. *Plasma Physics and Controlled Fusion*, 2018, 60 (3), pp.034005. 10.1088/1361-6587/aaa336 . hal-01717610

HAL Id: hal-01717610

<https://ensta-paris.hal.science/hal-01717610v1>

Submitted on 29 Oct 2024

HAL is a multi-disciplinary open access archive for the deposit and dissemination of scientific research documents, whether they are published or not. The documents may come from teaching and research institutions in France or abroad, or from public or private research centers.

L'archive ouverte pluridisciplinaire **HAL**, est destinée au dépôt et à la diffusion de documents scientifiques de niveau recherche, publiés ou non, émanant des établissements d'enseignement et de recherche français ou étrangers, des laboratoires publics ou privés.

PAPER

Numerical study of laser energy effects on density transition injection in laser wakefield acceleration

To cite this article: F Massimo *et al* 2018 *Plasma Phys. Control. Fusion* **60** 034005

View the [article online](#) for updates and enhancements.

Recent citations

- [Optical injection dynamics in two laser wakefield acceleration configurations](#)
Vojtech Horný *et al*




IOP | ebooks™

Bringing you innovative digital publishing with leading voices to create your essential collection of books in STEM research.

Start exploring the collection - download the first chapter of every title for free.

Numerical study of laser energy effects on density transition injection in laser wakefield acceleration

F Massimo¹ , A F Lifschitz¹, C Thaury¹ and V Malka^{1,2}

¹LOA, École Polytechnique, ENSTA ParisTech, CNRS, Université Paris-Saclay, 828 Bd des Maréchaux—91762 PALAISEAU Cedex, France

²Department of Physics of Complex Systems, Weizmann Institute of Science, Rehovot, 76100, Israel

E-mail: francesco.massimo@ensta-paristech.fr

Received 10 October 2017, revised 16 December 2017

Accepted for publication 20 December 2017

Published 24 January 2018



CrossMark

Abstract

Density transition (or *shock-front*) injection is a technique to obtain high quality electron beams in laser wakefield acceleration. This technique, which requires no additional laser pulse, is easy to implement and is receiving increasing interest. In addition to its performances, its setup realized with a blade inserted in a gas jet allows a certain flexibility in controlling the density transition shape, whose effects on the beam quality have been studied theoretically and experimentally. We report the results of particle-in-cell simulations where the laser energy is systematically varied for different shapes of the density transition. Our study shows how the laser energy affects the injection process, increasing the injected charge and influencing the other beam characteristics (e.g. energy and duration).

Keywords: plasma acceleration, laser plasma interaction, particle in cell

(Some figures may appear in colour only in the online journal)

1. Introduction

Laser wakefield acceleration (LWFA) [1–3] of electron beams produced in underdense plasmas represents a novel technology for compact sources of high quality electron beams, whose accelerating gradients exceeded by orders of magnitude those of conventional particle accelerators [4–7]. Applications for advanced radiation sources like free electron lasers (FEL) require high current, low energy spread and low emittance electron beams [8, 9]. Thus, the strong dependence of the final electron beam quality on the method used to inject them in the laser wakefield has motivated the investigation of injection techniques leading to increasingly higher beam qualities [3]. Particularly promising are the injection techniques involving tailoring of the plasma density profile [10–14]. In these techniques, the reduction of the wake phase velocity in a density downramp triggers injection of plasma electrons which move faster than the plasma wave [10].

In [12, 13], the injection of electrons through a sharp density transition (often called also *shock-front*) was reported, and the simple setup (a blade inserted in a gas jet) used to

manipulate the plasma density profile allowed to change the transition characteristics and thus the injected beam parameters. Such a technique can also be coupled to ionization injection [15–18], as demonstrated by Thaury *et al* [19]. The dependence of the beam parameters on the downramp length of the density transition and the beam evolution during the acceleration phase were theoretically studied and described thoroughly in [20]. The influence of both the density transition height and length in a *shock-front*-like profile were investigated afterwards [21]. A semi-analytical model to predict the injected beam length and the injection threshold in arbitrary downramps was then derived [22]. A study on the influence of the transition downramp steepness on the beam quality has then been presented in [23]. The studies in [20–23] employ different laser parameters, thus together they constitute a coherent but somewhat fragmented study of the density transition injection technique.

Compared to our previous work [21], where only the density transition parameters were varied, in this paper we expand the study, systematically varying both the density transition parameters, i.e. height and downramp length, as

well as the laser energy in a series of simulations and discuss how they change the final electron beam quality. We show how the laser energy strongly influences the injection and acceleration processes, thus completing our previous work.

The article is organized as follows. In the second section we introduce the numerical study. In the third section we discuss how the laser energy influences the beam characteristics, for various values of the density transition height and downramp length. In the fourth section we discuss how the laser energy changes the initial distribution of the injected electrons.

2. Parametric numerical study

As an extension of the study presented in [21], the simulation numerical parameters (briefly reported in the following) are the same as in that reference. Our simulations have been performed with the particle-in-cell (PIC) code CALDER-CIRC [24], which self-consistently evolves the macroparticles which sample the plasma distribution function in the 6D phase space and the electromagnetic fields (the laser pulse and the fields generated in the plasma). The code decomposes the electromagnetic fields in azimuthal modes with respect to the laser propagation direction. For our simulations we retained the first two modes, the most relevant for LWFA [24], and sampled the plasma with 50 macroparticles per mesh cell. Denoting with $\omega_0 = 2\pi c/\lambda$ the laser central frequency, we chose a resolution of $\Delta z = 0.2 c/\omega_0$ and $\Delta r = 0.9 c/\omega_0$ in the longitudinal and radial direction respectively and an integration timestep $\Delta t = 0.18 \omega_0^{-1}$.

The parameters of the reference laser pulse for our study are the same as in [21], i.e., based on the Ti:Sa laser system of Salle Jaune at Laboratoire d'Optique Appliquée (LOA): wavelength $\lambda = 0.8 \mu\text{m}$, FWHM duration 28 fs. The Gaussian laser pulse, linearly polarized along the y direction, has a waist size $w_0 = 12 \mu\text{m}$ at the entrance of an already ionized plasma, which has a plateau density of $n_0 = 3 \cdot 10^{18} \text{cm}^{-3}$. Given our laser wavelength and plasma density, the critical power for relativistic self-focusing [25] is equal to $P_c = 17.4(\lambda_p/\lambda) \text{GW} = 10^{-2} \text{PW}$. The laser pulse initial peak normalized potential is $a_0 = 2.5$, corresponding to a ratio between the total pulse power at waist and the critical power P_c of 3. The reference total energy of the laser pulse is thus 0.9 J. To investigate the influence of laser energy on the injection and acceleration, we varied the density profile peak and downramp length as in [21] and repeated the same simulations while decreasing and increasing the laser energy by 25%, varying only a_0 accordingly and keeping all the other laser parameters (waist size, duration) fixed.

The plasma density profile used for our simulations, depicted in figure 1 (solid surface), has a linear upramp of $L_{\text{upramp}} = 100 \mu\text{m}$, where the plasma density passes from zero to Kn_0 . After the density peak at $z = z_{\text{tp}} = 105 \mu\text{m}$, a linear downramp (where injection occurs) of length L_{down} decreases the density down to n_0 . This density profile is a simplified model of density transitions obtained through a

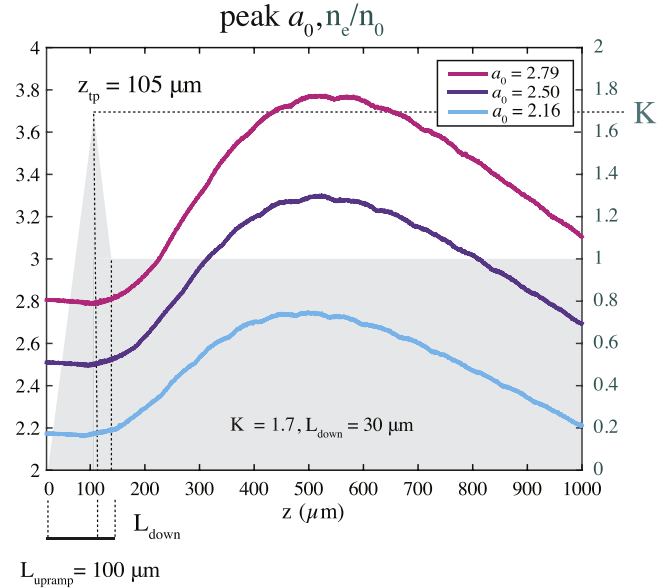


Figure 1. Filled surface with transparency: plasma density profile used in our study. The plasma density n_e is normalized by the plateau density n_0 . The plasma profile shown corresponds to a density transition with relative height $K = n_{e,\text{peak}}/n_0 = 1.7$, downramp length $L_{\text{down}} = 30 \mu\text{m}$. The laser propagates in the positive z direction. The density transition peak is located at $z_{\text{tp}} = 105 \mu\text{m}$. Our diagnostic point for the beam quality parameters corresponds to when the laser pulse reaches $z = 1 \text{mm}$. Curves: evolution of laser maximum vector potential a_0 during the propagation in the plasma, for $K = 1.7$, $L_{\text{down}} = 30 \mu\text{m}$. The values of a_0 reported in the legend are the initial peak vector potential of the laser.

blade in a gas jet [12–14, 19]. Following [26], the normalized phase velocity β_p of the wake in the downramp (i.e. $z_{\text{tp}} < z < z_{\text{tp}} + L_{\text{downramp}}$) is:

$$\beta_p = \frac{1}{1 + \frac{z - ct}{2n_e} \frac{dn_e}{dz}} \quad (1)$$

where the density n_e in the downramp is given by

$$n_e(z) = n_0 \left[K - \frac{K-1}{L_{\text{down}}} (z - z_{\text{tp}}) \right]. \quad (2)$$

From equation (1) it is clear that in the laser's wake ($z - ct < 0$), the wake phase velocity β_p can be lower than 1 in a density downramp ($\frac{dn_e}{dz} < 0$) and allow injection. An accurate estimate of β_p taking into account also the laser energy can be found in [22]. The simple estimate in equation (1) is given for the reader's convenience to compute quantities of interest as the injection or transit time [22].

The laser is injected from $z = 0 \mu\text{m}$ towards the z direction. Figure 1 also reports the evolution of the laser peak normalized potential from three simulations with $K = 1.7$, $L_{\text{down}} = 30 \mu\text{m}$ and increasing laser energies, $E = [0.675, 0.9, 1.125] \text{J}$, corresponding to a ratio between the total pulse power and the critical power $P/P_c = [2.25, 3.00, 3.25]$. For a given laser energy, changing K or L_{down} does not significantly alter the laser self-focusing.

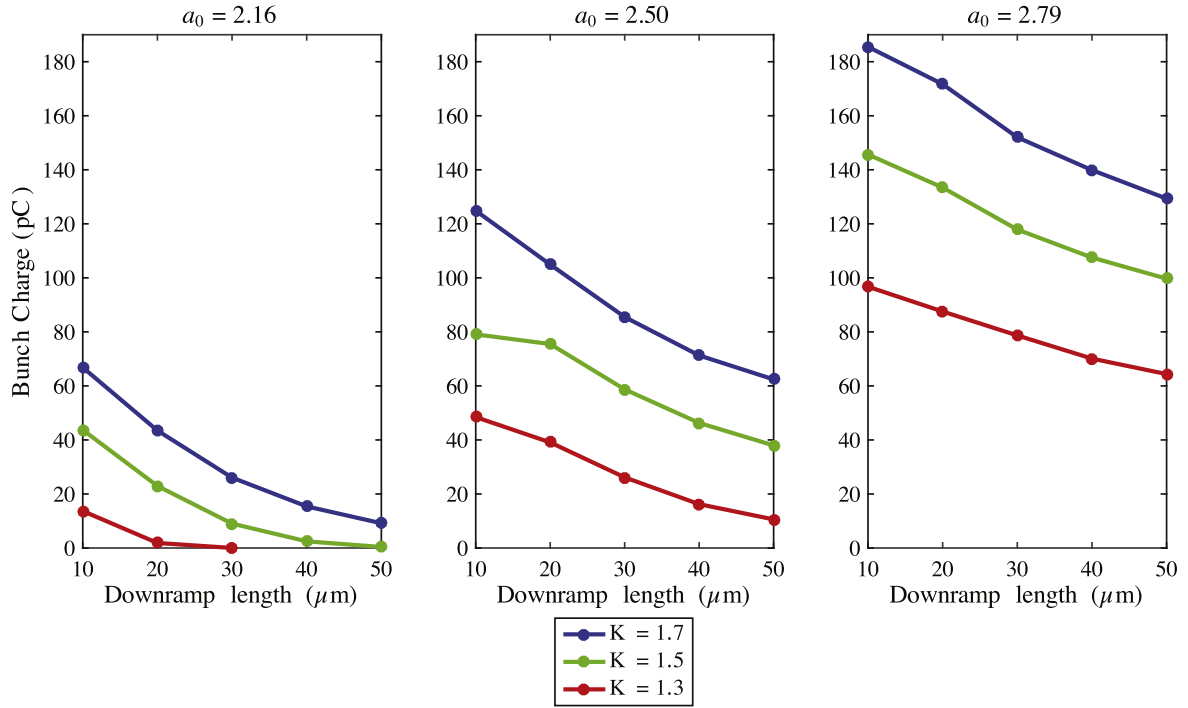


Figure 2. Variation of the beam injected charge with the density transition height K and downramp length L_{down} . The reported energy is evaluated $\approx 900 \mu\text{m}$ after the density transition peak. Each point represents the result of one simulation. The three panels refer to different values of the initial laser peak vector potential.

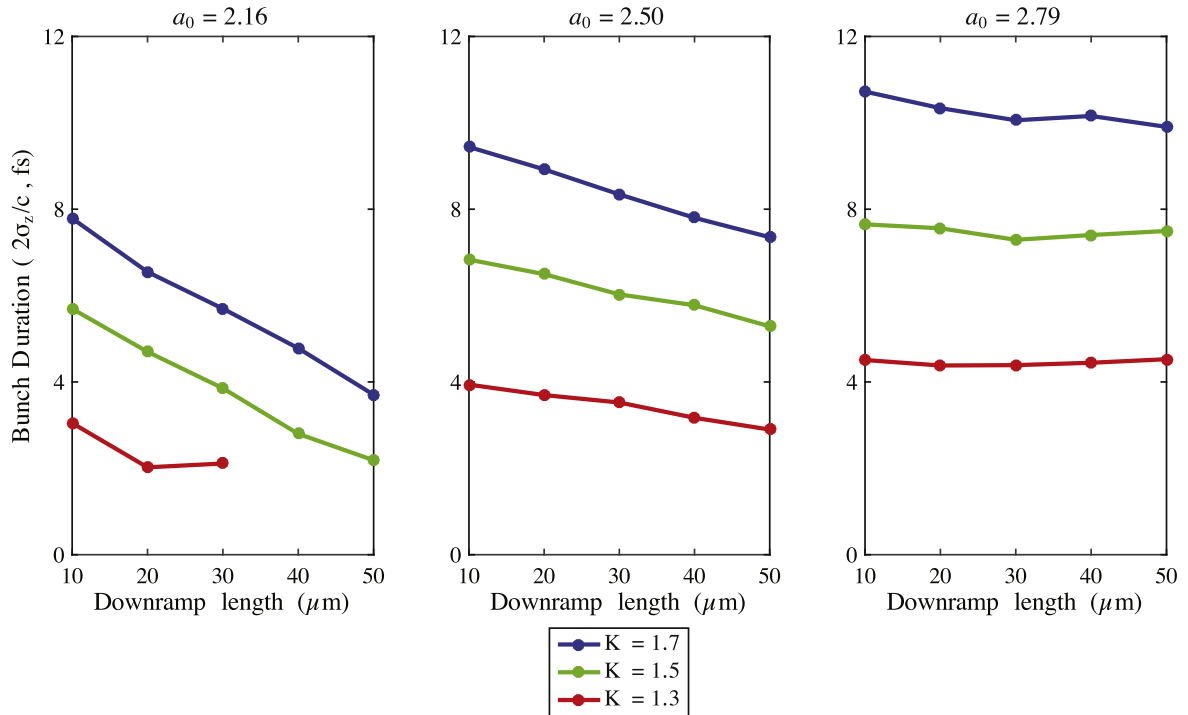


Figure 3. Variation of the beam duration (evaluated as twice the rms length in time) with the density transition height K and downramp length L_{down} . The reported duration is evaluated $\approx 900 \mu\text{m}$ after the density transition peak. Each point represents the result of one simulation. The three panels refer to different values of the initial laser peak vector potential.

Although satisfying the matched propagation condition $k_p w_0 = 2\sqrt{a_0}$ [27] would have guaranteed a more stable propagation of the laser pulse, the different values of a_0 used

in our study would have implied different values for the plateau density n_0 for a stable propagation. Instead, we preferred to isolate the effects of laser energy and of the

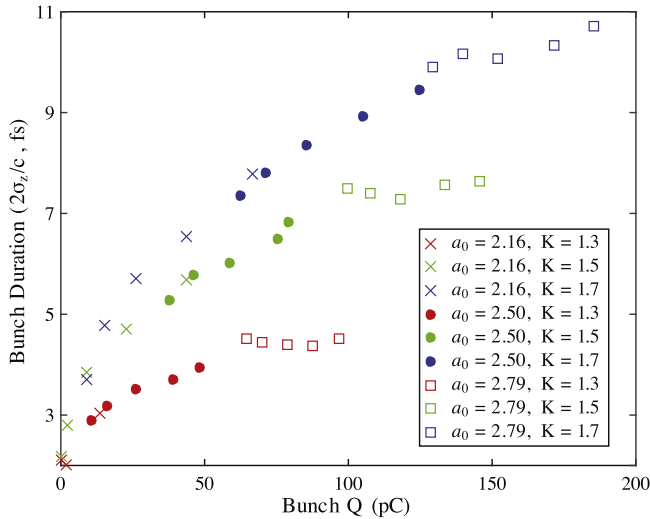


Figure 4. Variation of the beam duration with the beam charge. Cross, squares and circles denote different values of the initial laser peak vector potential, while the different colors represent different shock heights K . Each point represents the result of one simulation.

transition parameters. Thus, we kept fixed the plateau density to a value that does not trigger self-injection through relativistic self-focusing for all the considered laser energies.

3. Electron beam quality

The results of the parametric study are reported in the following. These simulations have as input the combinations of $K = [1.3, 1.5, 1.7]$, $L_{down} = [10, 20, 30, 40, 50] \mu\text{m}$ and laser energy $E = [0.675, 0.9, 1.125]$, corresponding to laser normalized potentials $a_0 = [2.16, 2.50, 2.79]$, with a fixed duration and waist size. For the sake of comparison, we remind that the results presented in [21] have been obtained with $a_0 = 2.5$, $K = [1.2, 1.3, 1.5]$, $L_{down} = [10, 20, 30, 40, 50] \mu\text{m}$. In all the simulations, the diagnostic on the electron beam parameters has been performed when the laser arrives at $z = 1\text{mm}$. For each electron beam parameter, three panels corresponding to increasing laser energy are displayed, to highlight the effects of different values of a_0 . Each point in the panels represents one of the performed simulations, with different colors representing different density transition heights: red curve $K = 1.3$, green curve $K = 1.5$, blue curve $K = 1.7$. No significant low energy tail was found in the energy spectrum of the electrons inside the wake bubble at the diagnostic point. Thus, for all the simulations, the electrons included in the calculation of the beam statistics are those well separated both in space and energy from the borders of the plasma bubble at the diagnostic point. Since the energy of the electrons in the wake was in general different for all the simulations, our inclusion criterion does not correspond to a threshold in energy or boundary in the position kept equal for all the simulations.

Figure 2 reports the total injected charge. As discussed in [20, 21], lower density transitions and/or longer downramps yield a lower injected charge. For $a_0 = 2.16$, $K = 1.3$ and for longer transitions ($L_{down} = 40, 50 \mu\text{m}$) no charge is injected; thus the points corresponding to those two simulations are absent also in the following figures. As expected, the laser energy plays a key role in the injection: lower values of a_0 yield a lower injected charge. Given a density transition shape, i.e. given K and L_{down} , the injected charge changes significantly with the laser energy. For example, for $K = 1.5$ and $L_{down} = 10 \mu\text{m}$, the charge drops by 50% and increases by 80% if the laser energy is respectively decreased and increased by 25%. For a given density transition, multiple effects affect the injected charge if the laser energy is changed. The wake phase velocity also depends on the laser a_0 in nonlinear regimes [22], thus the change in the wake phase velocity in the transition which triggers injection is influenced by the laser energy. Equivalently, the velocity threshold for the electrons to be injected is lowered when the laser peak field is increased. This effect, coupled with higher momenta of the electrons caused by higher accelerating gradients, increases the number of injected electrons with higher values of a_0 . Besides, in nonlinear regimes the wakefield bubble size increases with a_0 [28]. All these variations on the injection threshold, the electron momenta and the bubble size affect the injection volume in the downramp (as shown in section 4), greatly affecting the injected beam charge and duration with the laser energy.

Analogously, with higher energy the bunch duration increases and depends less and less on the downramp length, as can be seen from figure 3. A relation between the beam charge and its duration can be inferred from figure 4, where different K values form three monotonous curves in the beam charge-duration plane: given a value of K , beams with more charge tend to have a longer duration. We note that the linear dependence between beam charge and duration hinted in [22] is approximately valid with our density transition profile only with some combinations of a_0 , K and L_{down} . In general, given the density transition parameters, higher laser energies yield longer bunches, as the injection starts earlier in the downramp (see section 4).

For FEL amplification seeded by LWFA electron beams, peak currents of the order of a few kA are required [8, 9]. From figure 5, where the average current of the simulated beams is reported, the beam currents obtained are fully sufficient for most of the laser and density transition parameters. It is worth to note that with higher a_0 (see right panel), higher currents are obtained with lower relative peak density K . This is due to the rate of change of beam duration with injected charge at high a_0 (see figure 4).

The normalized emittances of the beam $\varepsilon_{n,i} = \sqrt{\sigma_i^2 \sigma_{p_i}^2 - \sigma_{i,p_i}^2}$ (σ_i , σ_{p_i} are respectively the standard deviation in transverse position and transverse momentum, σ_{i,p_i} is the correlation between transverse position and transverse momentum) in the planes $i = x, y$ are reported in figure 6.

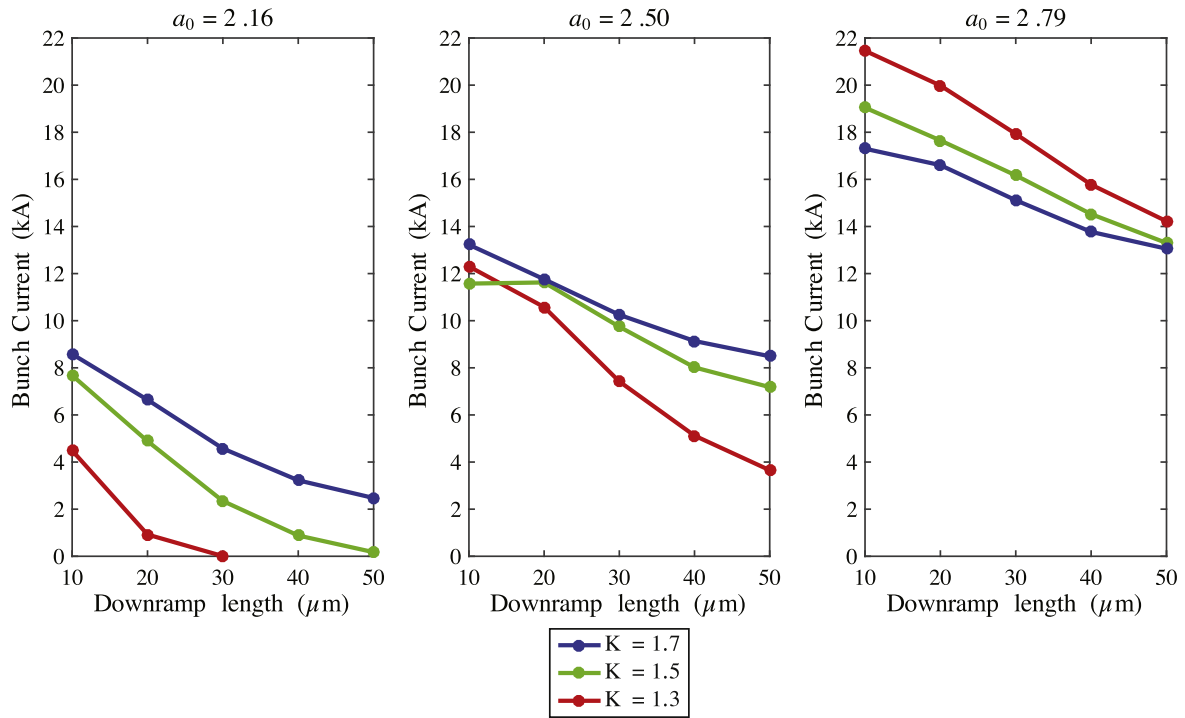


Figure 5. Variation of the beam average current (evaluated the charge divided by twice the rms length in time) with the density transition height K and downramp length L_{down} . The reported duration is evaluated $\approx 900 \mu\text{m}$ after the density transition peak. Each point represents the result of one simulation. The three panels refer to different values of the initial laser peak vector potential.

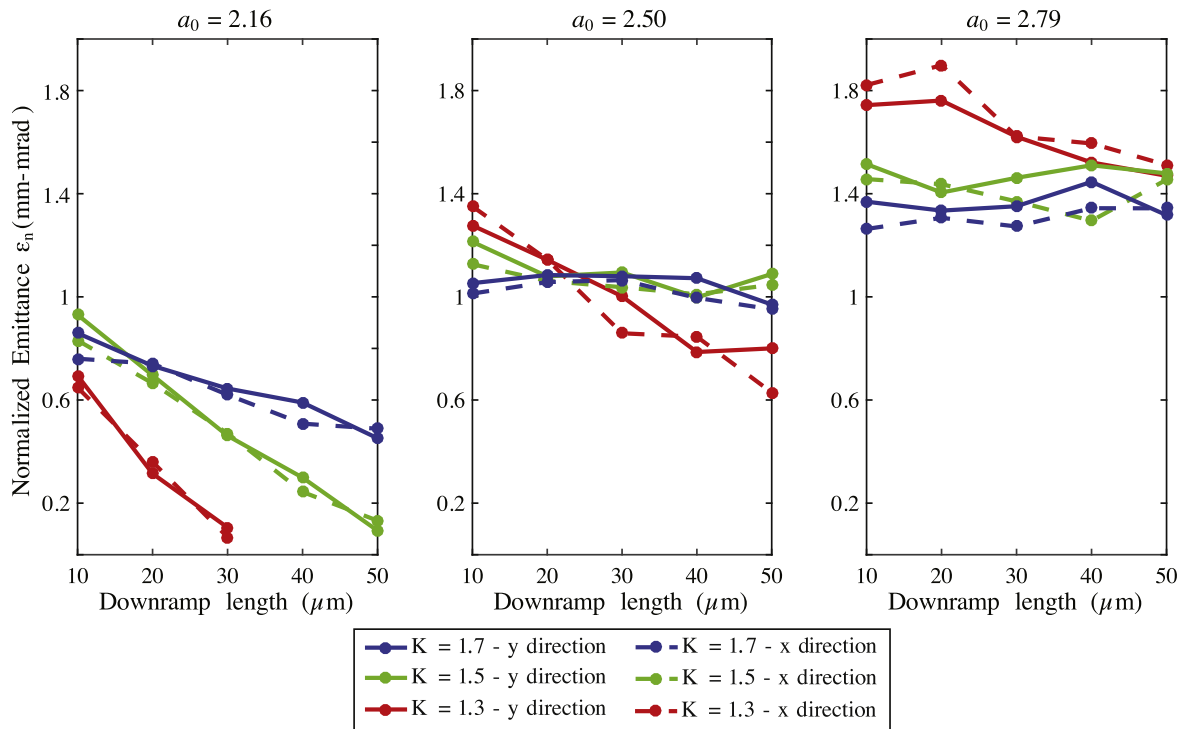


Figure 6. Variation of the beam normalized emittance with the density transition height K and downramp length L_{down} . The reported emittance is evaluated $\approx 900 \mu\text{m}$ after the density transition peak. Each point represents the result of one simulation. The three panels refer to different values of the initial laser peak vector potential.

The symmetry between the two transverse planes does not change with the laser energy, and also with $a_0 = 2.79$ the values of emittance are lower than 2 mm-mrad. Since our

simulations do not use an electromagnetic solver coping with numerical Cherenkov radiation (NCR) as the finite difference scheme presented in [29], our results provide an

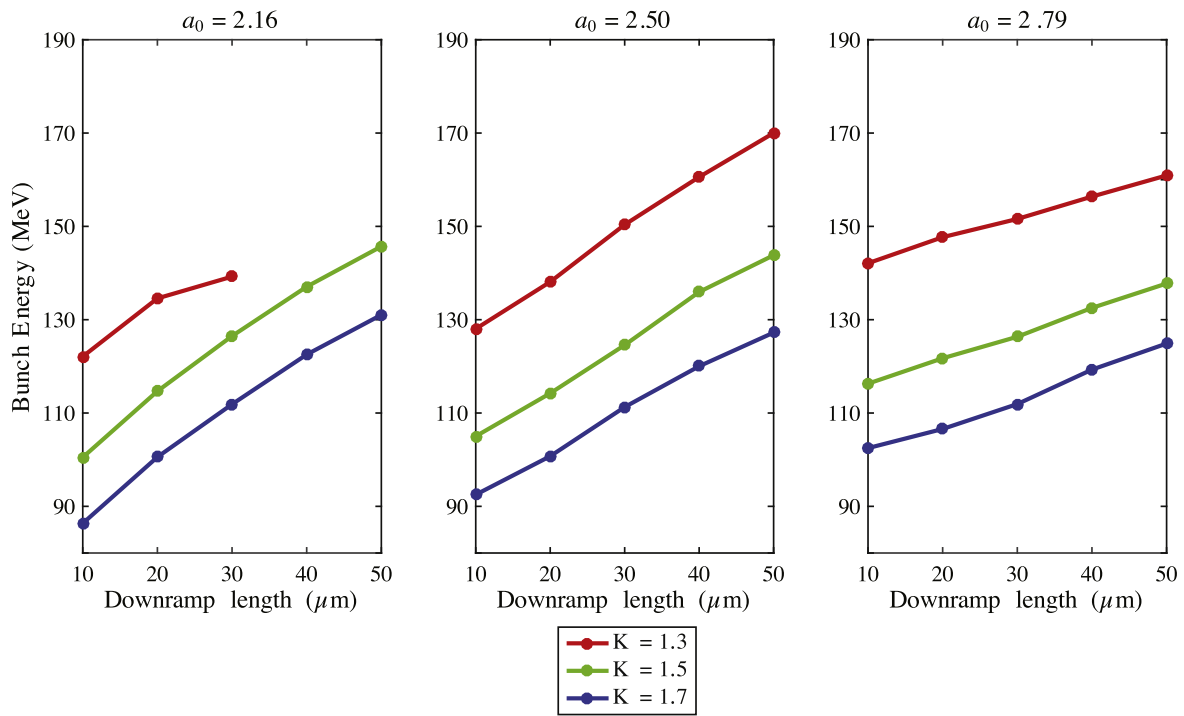


Figure 7. Variation of the beam energy with the density transition height K and downramp length L_{down} . The reported energy is evaluated $\approx 900 \mu\text{m}$ after the density transition peak. Each point represents the result of one simulation. The three panels refer to different values of the initial laser peak vector potential.

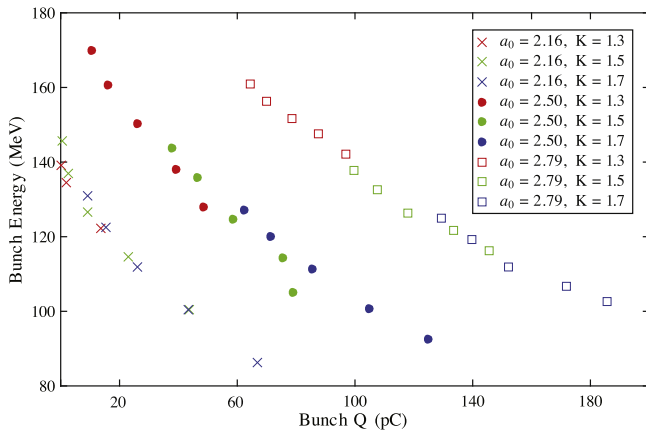


Figure 8. Variation of the beam energy with the beam charge. Cross, squares and circles denote different values of the initial laser peak vector potential, while the different colors represent different density transition heights K . Each point represents the result of one simulation. Five points are plotted for each couple (a_0, K) , corresponding to the five considered downramp lengths.

overestimation of the emittance, which normally is numerically increased by the NCR. The other beam parameters like charge and energy are normally not significantly affected by NCR [29].

Due to the beamloading, the increase in beam charge with a_0 prevents a sensitively higher energy gain. In figure 7

we report the mean beam energy. A higher energy could have been expected with a higher laser energy (the accelerating field is expected to scale with a_0), but the only effect rising with the laser energy, keeping fixed K and L_{down} , is a progressive insensitivity to L_{down} , shown also by the beam charge and duration. The higher a_0 yields a higher injected charge that compensates for the higher accelerating gradient with its field. Figure 8 illustrates the inverse correlation between injected charge and beam energy given a laser a_0 , a signature of beam loading [30]. Figure 8 shows also that for a given charge a higher energy can be obtained with higher a_0 .

Figure 9 reports the total rms energy spread of the beam. The final energy spread after acceleration is an interplay between various effects. From figure 9, it can be inferred that the beam energy spread strongly depends on the laser energy: a higher a_0 lowers the threshold for injection in the downramp, thus electrons with higher differences in energy are injected. In the second place, depending of how optimum is the deformation of the electric field distribution given by beam loading, different parts of the bunch could sample a similar or a sensitively different value of the accelerating field [31–33], thus maintaining stable or increasing the injected beam initial energy spread. From figure 4 and figure 9, beams with increasing duration, especially those from simulations with higher initial a_0 , tend to have higher energy spread. This can be caused by a higher deformation of the electric field distribution, by a higher charge and by a steeper accelerating

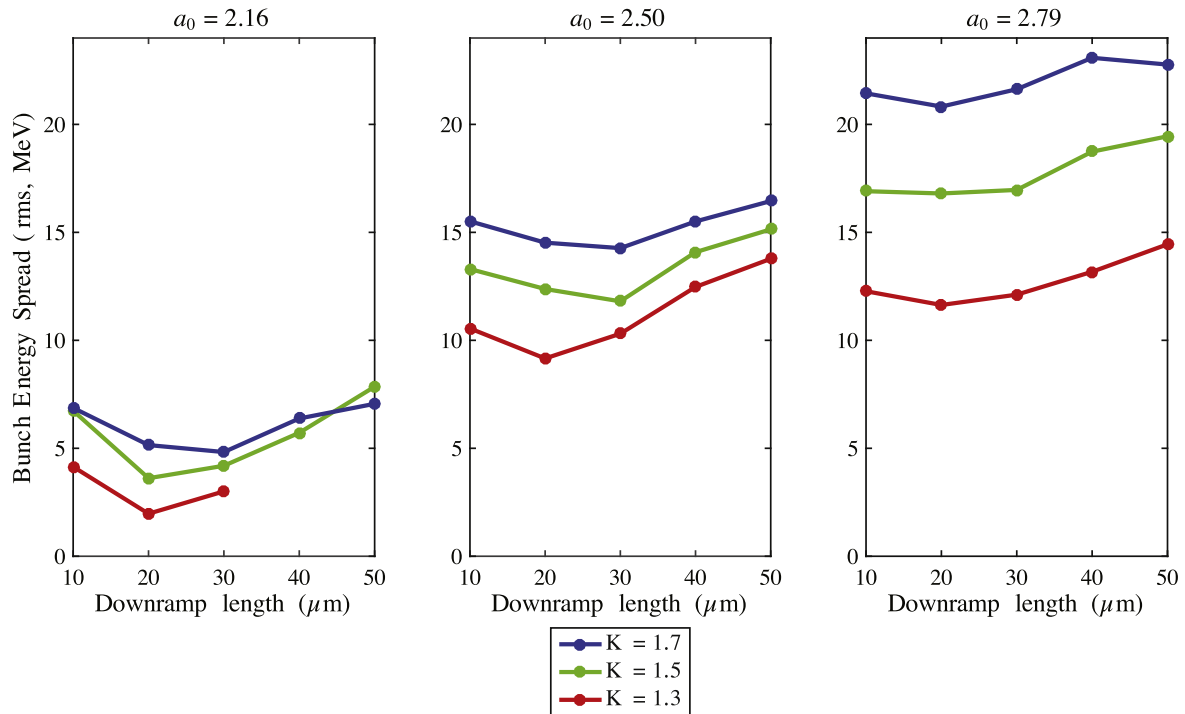


Figure 9. Variation of the beam rms energy spread with the density transition height K and downramp length L_{down} . The reported energy spread is evaluated $\approx 900 \mu\text{m}$ after the density transition peak. Each point represents the result of one simulation. The three panels refer to different values of the initial laser peak vector potential.

field difference between the head and the tail of the bunch. We remark that our analysis only considers energy spread values at $\approx 900 \mu\text{m}$ after the density transition peak. Different laser and density transition parameters can yield different evolutions for the beam energy spread during acceleration, and optimum accelerating distances may in principle be found [20].

The previously shown parameters are reported in table 1.

To give an intuitive, pictorial impression of the injection process, in figure 10 is depicted the electron density n_e at different timesteps for three simulations with same density transition parameters but increasing laser energy. From figure 10, the mentioned differences in bubble size and beam duration with different laser energies can be qualitatively inferred.

4. Laser energy effects on initial distribution of the injected electrons

Given the density transition parameters K and downramp length L_{down} , the laser energy influences the volume where the electrons are injected. As hinted in section 3, a higher a_0 increases the bubble size and influences the wake phase velocity change due to the density transition. The effects on the injection volume can be seen in figure 11 and figure 12 and summarized in table 2. Two example cases with different K and downramp length L_{down} , but similar charge, have been

chosen. Since the density transition parameters are fixed in each panel, the effects of the laser energy can be appreciated. In both cases, the injection volume is enlarged longitudinally and transversely with increasing a_0 , even more dramatically in the case of a longer downramp (figures 11, right panel). In the longitudinal plane, the injection starts earlier with higher laser energy, as more electrons gain enough momentum to be injected even at the beginning of the downramp, where the wake phase velocity decrease is lower [34]. Given the transition parameters, a longer injection volume due to higher laser energy increases the beam duration (see figure 3). In the transverse plane, we note that the difference in the density transition parameters do not significantly affect the initial charge distribution, while the laser energy has a more dramatic effect, enlarging transversally the injection volume with increasing a_0 . We note another transverse effect at higher energies: with shorter downramps (left panel) a sort of hole appears in the transverse initial distribution of the electrons. As shown in [35, 36], in a highly nonlinear regime the majority of electrons injected by self-injection come from a certain distance range from the laser propagation axis, which depends on the bubble radius. The density transition triggers a bubble enlargement similarly to the one triggering self-injection [35]. With longer downramps, a wider range of bubble transverse sizes during the laser propagation yields a more uniform distribution on the initial transverse position. Conversely, with a shorter downramp the bubble size value varies less, and less electrons are injected from near the axis.

Table 1. Variation of the beam charge Q , duration $2\sigma_z/c$, normalized transverse emittance $\varepsilon_{n,y-x}$, energy E , rms energy spread ΔE and average current I with laser initial normalized peak potential a_0 , the density transition height K and downramp length L_{down} . The reported quantities are evaluated $\approx 900 \mu\text{m}$ after the density transition peak.

$a_0 = 2.16$							
K	$L_{down} (\mu\text{m})$	Q (pC)	$2\sigma_z/c$ (fs)	$\varepsilon_{n,y-x}$ (mm-mrad)	E (MeV)	ΔE (MeV)	I (kA)
1.3	10	13.7	3.0	0.7-0.6	122.1	4.1	4.5
	20	1.8	2.0	0.3-0.3	134.6	2.0	0.9
	30	≈ 0	2.1	0.1-0.07	139.2	3.0	≈ 0
	40	0	—	—	—	—	—
	50	0	—	—	—	—	—
1.5	10	100.5	5.7	0.9-0.8	105	6.7	7.7
	20	114.7	4.7	0.7-0.7	114	3.6	4.9
	30	126.5	3.8	0.5-0.5	124	4.2	2.3
	40	137.1	2.8	0.3-0.2	136	5.7	0.9
	50	145.7	2.2	0.2-0.1	144	7.8	0.2
1.7	10	86.3	7.8	0.8-0.8	150	6.9	8.6
	20	100.6	6.5	0.7-0.7	160	5.1	6.6
	30	111.9	5.7	0.6-0.6	169	4.2	4.6
	40	122.5	4.8	0.6-0.5	176	6.4	3.2
	50	131.0	3.7	0.4-0.5	182	7.0	2.5
$a_0 = 2.50$							
K	$L_{down} (\mu\text{m})$	Q (pC)	$2\sigma_z/c$ (fs)	$\varepsilon_{n,y-x}$ (mm-mrad)	E (MeV)	ΔE (MeV)	I (kA)
1.3	10	48.4	3.9	1.4-1.4	128	10.5	12.3
	20	39.0	3.7	1.4-1.4	138	9.1	10.6
	30	26.1	3.5	1.2-1.1	150	10.3	7.4
	40	16.2	3.2	1.0-1.1	160	12.8	5.1
	50	10.6	2.3	0.7-0.6	170	13.8	3.6
1.5	10	79.1	6.8	1.3-1.3	105	13.3	11.6
	20	75.5	6.5	1.2-1.2	114	12.4	11.6
	30	58.7	6.0	1.2-1.2	124	11.8	9.7
	40	46.3	6.8	1.2-1.2	136	14.1	8.0
	50	38.0	5.3	1.1-1.1	144	15.1	7.2
1.7	10	124.9	9.4	1.0-1.0	92	15.5	13.2
	20	104.9	8.9	1.1-1.0	101	14.5	11.7
	30	85.5	8.3	1.1-1.1	111	14.3	10.2
	40	71.3	7.8	1.1-1.0	120	15.5	9.1
	50	62.4	7.3	1.0-1.0	127	16.4	8.5
$a_0 = 2.79$							
K	$L_{down} (\mu\text{m})$	Q (pC)	$2\sigma_z/c$ (fs)	$\varepsilon_{n,y-x}$ (mm-mrad)	E (MeV)	ΔE (MeV)	I (kA)
1.3	10	96.7	4.5	1.7-1.8	142.1	12.3	21.4
	20	87.5	4.4	1.8-1.9	147.7	11.6	20.0
	30	78.7	4.4	1.6-1.6	151.6	12.1	17.9
	40	70.1	4.4	1.5-1.6	156.4	13.1	15.8
	50	64.4	4.5	1.5-1.5	160.9	14.4	14.3
1.5	10	145.7	7.6	1.5-1.4	116.3	16.9	19.0
	20	133.4	7.5	1.4-1.4	121.7	16.8	17.6
	30	117.9	7.3	1.5-1.4	126.3	17.0	16.2
	40	107.5	7.4	1.5-1.3	132.5	18.7	14.5
	50	99.7	7.5	1.5-1.4	137.7	19.4	13.3
1.7	10	185.5	10.7	1.4-1.3	102.5	21.4	17.3
	20	171.7	10.3	1.3-1.3	106.6	20.8	16.6
	30	152.0	10.0	1.3-1.3	111.9	21.6	15.1
	40	139.9	10.1	1.4-1.3	119.3	23.0	13.8
	50	129.3	9.9	1.3-1.3	124.9	22.8	13.0

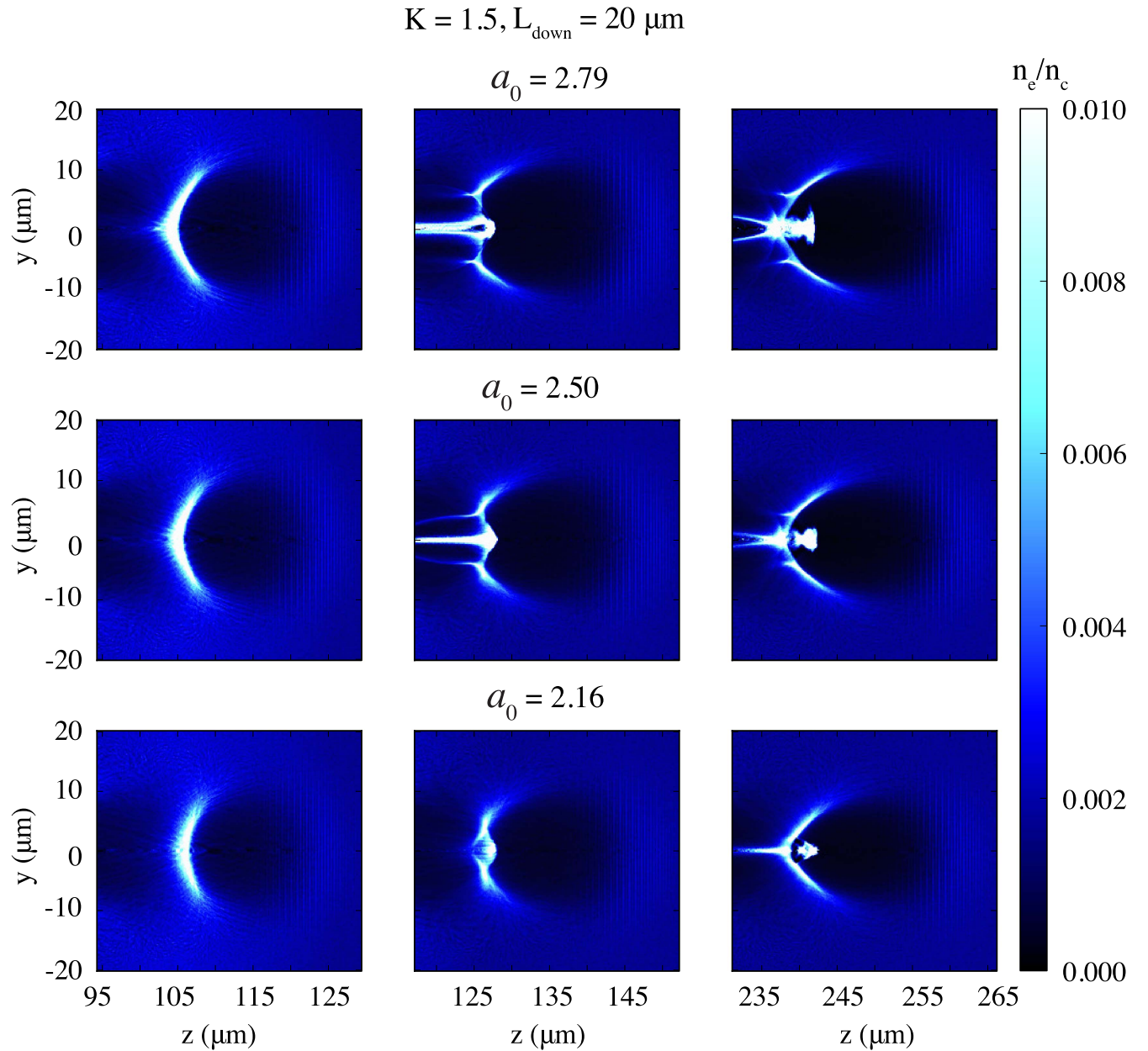


Figure 10. Injection process with a density transition with relative height $K = 1.5$, downramp length $L_{\text{down}} = 20 \mu\text{m}$, with different values for the initial laser peak vector potential: $a_0 = 2.79$ (top row panels), $a_0 = 2.50$ (middle row panels), $a_0 = 2.16$ (bottom row panels). The injection process is shown with snapshots of the electron density at times when the wake bubble tail is approximately at the position of the density transition peak $z = z_{\text{tp}} = 105 \mu\text{m}$ (left column panels), approximately at the end of the downramp $z = 125 \mu\text{m}$ (central column panels), at $z \approx 240 \mu\text{m}$ (right column panels).

5. Conclusions

In this paper we reported the results of PIC simulations of density transition (or *shock-front*) injection, which extend our previous study [21] where we varied the density transition parameters. Our investigation gives a wide picture of the effects of the plasma and laser parameters in this injection method. In our present study, we varied the laser peak vector potential a_0 , to highlight the effects of laser energy. For this

purpose, we computed the beam parameters after $\approx 1\text{mm}$. Increasing the laser energy increases the injected charge, at expenses of the final beam quality in terms of energy spread, duration and normalized emittance. The increase of the laser energy does not significantly increase the beam final energy at a given distance, due to the beamloading brought by a higher injected charge. However, a higher-energy laser is depleted at longer distances, thus higher given energy may eventually be obtained in principle.

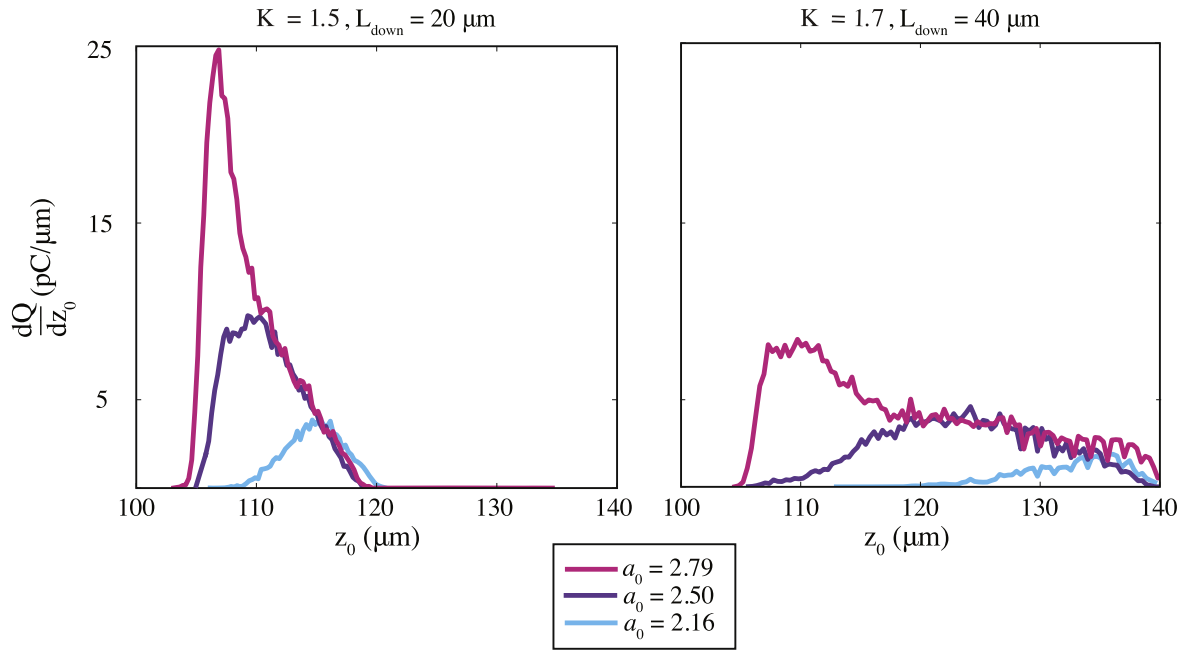


Figure 11. Left panel: charge distribution $\frac{dQ}{dz_0}$ with respect to the initial longitudinal coordinate z_0 of the injected electrons in the simulations corresponding to $K = 1.5$ and $L_{down} = 20 \mu\text{m}$. Right panel: charge distribution $\frac{dQ}{dz_0}$ with respect to the initial longitudinal coordinate z_0 of the injected electrons in the simulations corresponding to $K = 1.7$ and $L_{down} = 40 \mu\text{m}$.

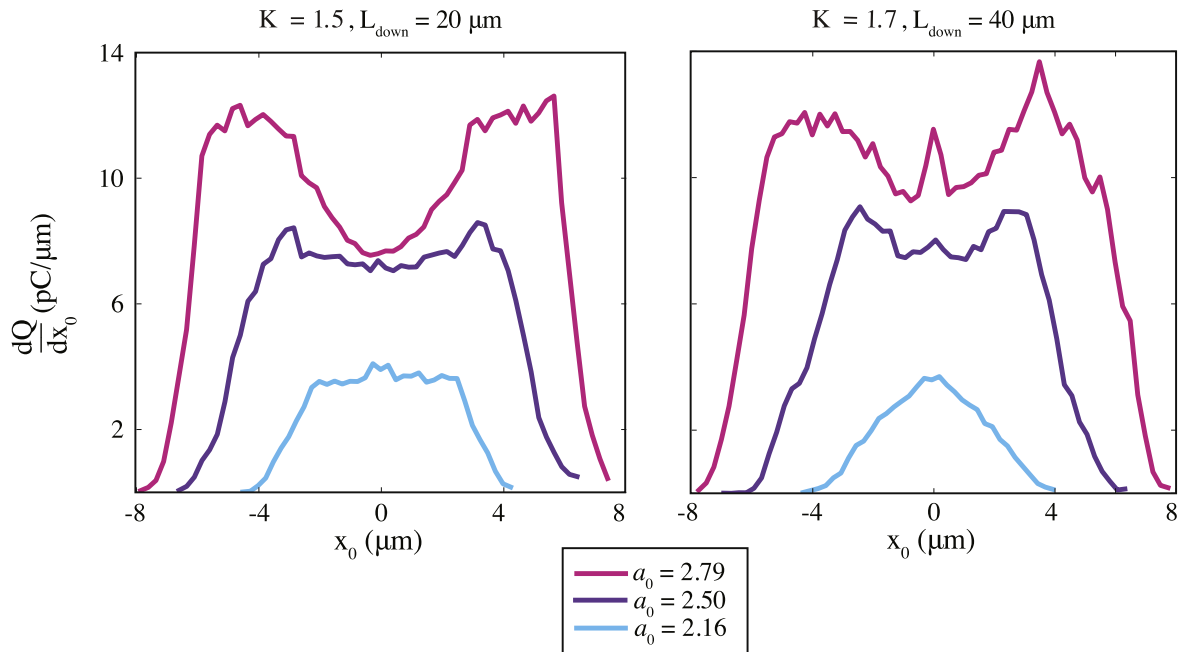


Figure 12. Left panel: charge distribution $\frac{dQ}{dx_0}$ with respect to the initial transverse coordinate x_0 of the injected electrons in the simulations corresponding to $K = 1.5$ and $L_{down} = 20 \mu\text{m}$. Right panel: charge distribution $\frac{dQ}{dx_0}$ with respect to the initial transverse coordinate x_0 of the injected electrons in the simulations corresponding to $K = 1.7$ and $L_{down} = 40 \mu\text{m}$.

Table 2. Average \bar{z}_0 and rms spread σ_{z_0} , σ_{x_0} of the charge distribution with respect to the initial coordinates z_0 and x_0 of the injected electrons in the simulations corresponding to $K = 1.3, 1.5$ and $L_{down} = 20, 50$, for different initial laser peak vector potential a_0 . The reported charge distributions have been evaluated considering the initial positions of the particles; to highlight this, the axes have been relabeled as z_0, x_0 .

a_0	K	L_{down} (μm)	Q (pC)	\bar{z}_0 (μm)	σ_{z_0} (μm)	σ_{x_0} (μm)
2.16	1.5	20	23	114.8	2.4	1.9
2.50	1.5	20	75	110.8	2.9	3.0
2.79	1.5	20	133	109.2	3.1	3.9
2.16	1.7	40	15	132.5	4.3	1.6
2.50	1.7	40	71	123.6	6.7	2.7
2.79	1.7	40	140	118.9	9.3	3.8

Acknowledgments

The authors acknowledge the support by the European Unions Horizon 2020 research and innovation programme under grant agreement EuPRAXIA No. 653782, European Union's Horizon 2020 Research and Innovation programme under Grant Agreement No 730871 and X-Five ERC project, contract No. 339128. This work was granted access to the HPC resources of TGCC under the allocation 2017—A0010510062 made by GENCI.

ORCID iDs

F Massimo  <https://orcid.org/0000-0002-5686-2537>

References

- [1] Tajima T and Dawson J M 1979 Laser electron accelerator *Phys. Rev. Lett.* **43** 267–70
- [2] Esarey E, Schroeder C B and Leemans W P 2009 Physics of laser-driven plasma-based electron accelerators *Rev. Mod. Phys.* **81** 1229–85
- [3] Malka V 2012 Laser plasma accelerators *Phys. Plasmas* **19** 055501
- [4] Malka V *et al* 2002 Electron acceleration by a wake field forced by an intense ultrashort laser pulse *Science* **298** 1596–600
- [5] Mangles S P D *et al* 2004 Monoenergetic beams of relativistic electrons from intense laser-plasma interactions *Nature* **431** 535–8
- [6] Geddes C G R, Toth Cs, van Tilborg J, Esarey E, Schroeder C B, Bruhwiler D, Nieter C, Cary J and Leemans W P 2004 High-quality electron beams from a laser wakefield accelerator using plasma-channel guiding *Nature* **431** 538–41
- [7] Faure J, Glinec Y, Pukhov A, Kiselev S, Gordienko S, Lefebvre E, Rousseau J P, Burgy F and Malka V 2004 A laser-plasma accelerator producing monoenergetic electron beams *Nature* **431** 541–4
- [8] Corde S, Ta Phuoc K, Lambert G, Fitour R, Malka V, Rousse A, Beck A and Lefebvre E 2013 Femtosecond x rays from laser-plasma accelerators *Rev. Mod. Phys.* **85** 1–48
- [9] Couprie M E *et al* 2016 An application of laser-plasma acceleration: towards a free-electron laser amplification *Plasma Phys. Control. Fusion* **58** 034020
- [10] Bulanov S, Naumova N, Pegoraro F and Sakai J 1998 Particle injection into the wave acceleration phase due to nonlinear wake wave breaking *Phys. Rev. E* **58** R5257–60
- [11] Faure J, Rechatin C, Lundh O, Ammoura L and Malka V 2010 Injection and acceleration of quasimonoenergetic relativistic electron beams using density gradients at the edges of a plasma channel *Phys. Plasmas* **17** 083107
- [12] Schmid K, Buck A, Sears C M S, Mikhailova J M, Tautz R, Herrmann D, Geissler M, Krausz F and Weisz L 2010 Density-transition based electron injector for laser driven wakefield accelerators *Phys. Rev. ST Accel. Beams* **13** 091301
- [13] Buck A *et al* 2013 Shock-front injector for high-quality laser-plasma acceleration *Phys. Rev. Lett.* **110** 185006
- [14] Hansson M, Aurand B, Davoine X, Ekerfelt H, Svensson K, Persson A, Wahlström C-G and Lundh O 2015 Down-ramp injection and independently controlled acceleration of electrons in a tailored laser wakefield accelerator *Phys. Rev. ST Accel. Beams* **18** 071303
- [15] McGuffey C *et al* 2010 Ionization induced trapping in a laser wakefield accelerator *Phys. Rev. Lett.* **104** 025004
- [16] Pak A, Marsh K A, Martins S F, Lu W, Mori W B and Joshi C 2010 Injection and trapping of tunnel-ionized electrons into laser-produced wakes *Phys. Rev. Lett.* **104** 025003
- [17] Pollock B B *et al* 2011 Demonstration of a narrow energy spread, 0.5 gev electron beam from a two-stage laser wakefield accelerator *Phys. Rev. Lett.* **107** 045001
- [18] Golovin G, Chen S, Powers N, Liu C, Banerjee S, Zhang J, Zeng M, Sheng Z and Umstadter D 2015 Tunable monoenergetic electron beams from independently controllable laser-wakefield acceleration and injection *Phys. Rev. ST Accel. Beams* **18** 011301
- [19] Thauray C *et al* 2015 Shock assisted ionization injection in laser-plasma accelerators *Sci. Rep.* **5** 16310 EP–, 11
- [20] Samant S A, Upadhyay A K and Krishnagopal S 2014 High brightness electron beams from density transition laser wakefield acceleration for short-wavelength free-electron lasers *Plasma Phys. Control. Fusion* **56** 095003
- [21] Massimo F, Lifschitz A F, Thauray C and Malka V 2017 Numerical studies of density transition injection in laser wakefield acceleration *Plasma Phys. Control. Fusion* **59** 085004
- [22] Tooley M P, Ersfeld B, Yoffe S R, Noble A, Brunetti E, Sheng Z M, Islam M R and Jaroszynski D A 2017 Towards attosecond high-energy electron bunches: Controlling self-injection in laser-wakefield accelerators through plasma-density modulation *Phys. Rev. Lett.* **119** 044801
- [23] Ekerfelt H, Hansson M, González I G, Davoine X and Lundh O 2017 A tunable electron beam source using trapping of electrons in a density down-ramp in laser wakefield acceleration *Sci. Rep.* **7** 12229
- [24] Lifschitz A, Davoine X, Lefebvre E, Faure J, Rechatin C and Malka V 2008 Particle-in-Cell modelling of laser-plasma interaction using Fourier decomposition *J. Comput. Phys.* **228** 1803–14
- [25] Sprangle P, Tang C-M and Esarey E 1987 Relativistic self-focusing of short-pulse radiation beams in plasmas *IEEE Trans. Plasma Sci.* **15** 145
- [26] Fubiani G, Esarey E, Schroeder C B and Leemans W P 2006 Improvement of electron beam quality in optical injection schemes using negative plasma density gradients *Phys. Rev. E* **73** 026402

- [27] Lu W, Tzoufras M, Joshi C, Tsung F S, Mori W B, Vieira J, Fonseca R A and Silva L O 2007 Generating multi-gev electron bunches using single stage laser wakefield acceleration in a 3d nonlinear regime *Phys. Rev. ST Accel. Beams* **10** 061301
- [28] Benedetti C, Schroeder C B, Esarey E, Rossi F and Leemans W P 2013 Numerical investigation of electron self-injection in the nonlinear bubble regime *Phys. Plasmas* **20** 103108
- [29] Lehe R, Lifschitz A, Taury C, Malka V and Davoine X 2013 Numerical growth of emittance in simulations of laser-wakefield acceleration *Phys. Rev. ST Accel. Beams* **16** 021301
- [30] Rechatin C, Davoine X, Lifschitz A, Ben Ismail A, Lim J, Lefebvre E, Faure J and Malka V 2009 Observation of beam loading in a laser-plasma accelerator *Phys. Rev. Lett.* **103** 194804
- [31] Tzoufras M, Lu W, Tsung F S, Huang C, Mori W B, Katsouleas T C, Vieira J, Fonseca R A and Silva L O 2008 Beam loading in the nonlinear regime of plasma-based acceleration *Phys. Rev. Lett.* **101** 145002
- [32] Tzoufras M, Lu W, Tsung F S, Huang C, Mori W B, Katsouleas T, Vieira J, Fonseca R A and Silva L O 2009 Beam loading by electrons in nonlinear plasma wakes *Phys. Plasmas* **16** 056705
- [33] Rechatin C *et al* 2010 Characterization of the beam loading effects in a laser plasma accelerator *New J. Phys.* **12** 045023
- [34] Xu X L, Li F, An W, Dalichaouch T N, Yu P, Lu W, Joshi C and Mori W B 2017 High quality electron bunch generation using a longitudinal density-tailored plasma-based accelerator in the three-dimensional blowout regime *Phys. Rev. Accel. Beams* **20** 111303
- [35] Kalmykov S, Yi S A, Khudik V and Shvets G 2009 Electron self-injection and trapping into an evolving plasma bubble *Phys. Rev. Lett.* **103** 135004
- [36] Wu H-C, Xie B-S, Liu M-P, Hong X-R, Zhang S and Yu M Y 2009 Electron trajectories and betatron oscillation in the wake bubble in laser-plasma interaction *Phys. Plasmas* **16** 073108